TotalControl

Advanced integrated supervisory and wind turbine control for optimal operation of large Wind Power Plants

Flow Database for reference wind farms
part 1: precursor simulations
D1.04

Delivery date: 30.04.2019

Lead beneficiary: KU Leuven

Dissemination level: Public

This project has received funding from the European Union's Horizon 2020 Research and Innovation Programme under grant agreement No. 727680

Author(s) information (alphabetical):		
Name	Organisation	Email
Søren Juhl Andersen	DTU	sjan@dtu.dk
Johan Meyers	KU Leuven	johan.meyers@kuleuven.be
Wim Munters	KU Leuven	wim.munters@kuleuven.be
Ishaan Sood	KU Leuven	ishaan.sood@kuleuven.be
Niels Troldborg	DTU	niet@dtu.dk

Document information

Version	Date	Description			
			Prepared by	Reviewed by	Approved by
1	29.04.2019	Name	Wim Munters	Johan Meyers	
2	30.04.2019	Name	Søren Juhl Andersen, Niels Troldborg		
3	02.05.2019	Name	Johan Meyers		Johan Meyers

TABLE OF CONTENTS

1. EXECUTIVE SUMMARY

One of the core activities within the TotalControl project is the development and validation of appropriate end-to-end wind-farm simulation models that cover the whole chain from flow model over aero-elastic model to power-grid model. Proper validation of control- and design-oriented engineering models requires accurate reference data. In addition to the available field measurement data, which in practice tend to be sparse and case-specific, high-fidelity large-eddy simulation (LES) tools provide a virtual wind-farm environment from which rich numerical measurements can be taken under controlled conditions.

The current report discusses the generation of atmospheric-boundary-layer flow data without turbines (so-called precursor simulations). This data can e.g. be used as input data for an offline aero-elastic model, as a way of characterizing incoming atmospheric flow conditions, or as dynamic turbulent inflow conditions for wind-farm simulations. The data is generated using two independent large-eddy simulation codes. The simulation cases can be categorized into two groups: a set of canonical pressure-driven boundary layers and a set of atmospheric boundary layers with neutral stratification and a capping inversion on top (so-called conventionally neutral boundary layers). Subsets of the generated data have been made publicly available and further data is available upon request.

2. INTRODUCTION

One of the core activities within the TotalControl project is the development and validation of appropriate end-to-end wind-farm simulation models that cover the whole chain from flow model over aero-elastic model to power-grid model. Proper validation of control- and design-oriented engineering models requires accurate reference data. In addition to the available field measurement data, which in practice tends to be sparse and case-specific, high-fidelity large-eddy simulation (LES) tools provide a virtual wind-farm environment from which rich numerical measurements can be taken under controlled conditions. In this regard, a high-fidelity reference database is generated using two independent numerical platforms.

The data included in the TotalControl flow database consists of two parts. The first part (further denoted as precursor data) contains unsteady three-dimensional flow data of an unperturbed atmospheric boundary layer (i.e. without the influence of turbines). This data can e.g. be used as input data for an offline aero-elastic model, or as a way of characterizing incoming atmospheric flow conditions. The second part contains similar data obtained from simulations including turbines. The inlet conditions of the latter simulations are derived from the precursor data itself. Data from this second part can e.g. be used to characterize and benchmark wake interaction, power extraction, and turbine loading within a wind farm. The current document focuses on the first part, i.e. the precursor data of atmospheric boundary layer simulations without any turbines. The wind-farm data will be discussed in a follow-up document that is estimated to appear at the end of 2019 (i.e. Month 24 of the TotalControl project).

The atmospheric conditions of the simulation cases have been designed through a series of discussions between the authors of this document. The cases can be divided into two main categories: on the one hand, canonical pressure-driven boundary layer cases are used as a simplified surrogate for a neutral atmospheric boundary layer; on the other hand, actual atmospheric boundary layers with a conventionally neutral stratification are simulated, i.e. including Coriolis and buoyancy forces. A parameter sweep covers different turbulence intensities and boundary layer heights.

The document is outlined as follows. First, a brief review of the reference wind farms considered in TotalControl is given. Then, the canonical pressure-driven boundary layer cases are outlined and general flow statistics are shown. Next, the same is done for the conventionally-neutral atmospheric boundary layer flow cases. Finally, the document is concluded with a detailed description of the dataset availability and general scripts to load in the data files.

3. TOTALCONTROL REFERENCE WIND POWER PLANT

The TotalControl Reference Wind Power Plant (TC RWP) has been defined in deliverable D1_03 of TotalControl (see Andersen et al. 2018). The TC RWP consists of 32 turbines in a staggered pattern, see *Figure 1*. The choice of a staggered pattern is somewhat arbitrary; but it makes sense to arrange the turbines in this manner if the prevailing wind direction were from the left. The reference turbines are the DTU 10 MW turbines (Bak et al., 2013), with a hub height of 119 m and a rotor diameter of 198 m.

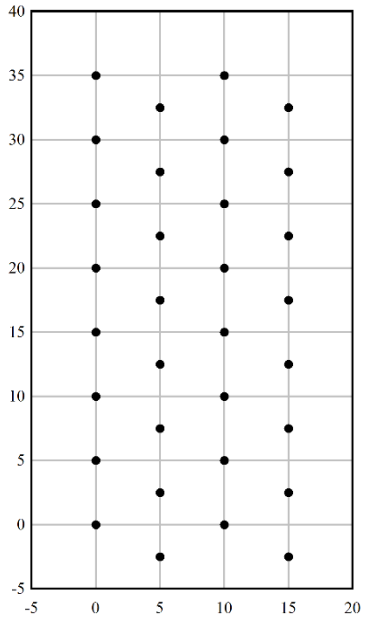

Figure 1: Layout of the TC RWP. Axes have units of s/D, with a rotor diameter D = 198 m.

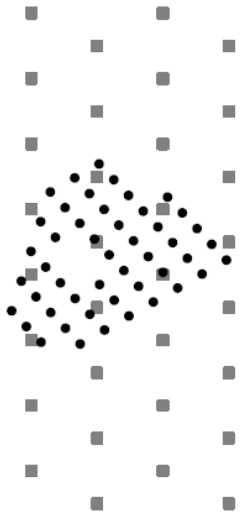

Figure 2: Scale comparison of the TC RWP (gray) and the Lillgrund WP (black)

The number of turbines results from a compromise between limiting the computational cost of high-resolution flow simulations and having an array that is large enough to be relevant as an offshore wind power plant. *Figure 2* shows a scale comparison of the TC RWP to the Lillgrund plant, also featured in the TotalControl project.

The columns of eight turbines (vertical in *Figure 1*) provide a "long" direction. When the wind is in this direction, the turbine-to-turbine wake effects can approach their asymptotic values. Furthermore, given a top-down wind direction a typical aligned layout is achieved, for which wake redirection was found to be a very efficient wind-farm control strategy (Munters and Meyers 2018). In the perpendicular "short" direction (horizontal in *Figure 1*) only two turbines are directly aligned. For a left-right wind direction, a standard staggered configuration is achieved, for which wake induction control strategies have been found to be more suitable. In this way, both the redirection and induction approach to wind-farm control can be investigated without a priori favouring one over the other based on wind-farm layout.

4. VIRTUAL WIND FARM ENVIRONMENT

The virtual wind farm environment used for generating the flow database consists of two independent numerical solvers, each with their own characteristics, solving the same governing equations for atmospheric boundary-layer flow. Firstly, the governing equations are detailed, and afterwards the SP-Wind and EllipSys 3D numerical solvers are discussed.

4.1. GOVERNING EQUATIONS

All simulations are based on the three-dimensional, unsteady, and spatially filtered Navier–Stokes momentum and temperature equations

$$\nabla \cdot \widetilde{\boldsymbol{u}} = 0$$

$$\frac{\partial \widetilde{\boldsymbol{u}}}{\partial t} + (\widetilde{\boldsymbol{u}} \cdot \nabla)\widetilde{\boldsymbol{u}} = -\frac{\nabla(\tilde{p} + p_\infty)}{\rho} - \nabla \cdot \boldsymbol{\tau}_s + 2\boldsymbol{\Omega} \times \widetilde{\boldsymbol{u}} + \boldsymbol{g}\left(\tilde{\theta} - \theta_0\right)/\theta_0 + \boldsymbol{\tau}_w + \boldsymbol{f}$$

$$\frac{\partial \tilde{\theta}}{\partial t} + (\widetilde{\boldsymbol{u}} \cdot \nabla)\tilde{\theta} = -\nabla \cdot \boldsymbol{q}_s$$

which are solved by means of Large-Eddy Simulation. In these equations, $\widetilde{\boldsymbol{u}}$ and $\tilde{p}$ are the filtered velocity and pressure fields respectively. Further, $\tilde{\theta}$ is the filtered potential temperature field, and θ_0 is the background adiabatic base state. The pressure gradient is readily split into a background pressure gradient ∇p_∞ driving the mean flow, and a fluctuating component $\nabla \tilde{p}$. The very high Reynolds numbers in atmospheric boundary-layer flows combined with typical spatial resolutions in LES justify the omission of resolved effects of viscous momentum transfer and diffusive heat transfer. Instead, these are represented by modeling the subgrid-scale stress tensor $\boldsymbol{\tau}_s$ and the subgrid-scale heat flux $\boldsymbol{q}_s$ originating from spatially filtering the original governing equations. Coriolis effects are included through the Earth's angular velocity vector $\boldsymbol{\Omega}$, and thermal buoyancy is represented by $\boldsymbol{g}(\theta - \theta_0)/\theta_0$, with $\boldsymbol{g}$ the gravitational acceleration, $\tilde{\theta}$ the filtered potential temperature and θ_0 a reference temperature. The effect of the sea surface is included using a rough-wall stress boundary $\boldsymbol{\tau}_w$, corresponding to a logarithmic velocity profile with a roughness length z_0. Finally, $\boldsymbol{f}$ represents any remaining body forces (e.g. by wind turbines) on the flow.

4.2. SIMULATION PLATFORMS

Simulations are performed by KU Leuven (using SP-Wind), and by DTU (using EllipSys3D). A short description of these simulation platforms is given below.

4.2.1. SP-WIND (KU LEUVEN)

SP-Wind is a wind-farm LES code built on a high-order flow solver developed over the last 12 years at KU Leuven (Calaf, Meneveau & Meyers 2010; Munters, Meneveau & Meyers 2016; Allaerts & Meyers 2017). Spatial discretization is performed by combining pseudo-spectral schemes with fourth-order energy-conservative finite differences. The equations are marched in time using a fully explicit fourth-order Runge-Kutta scheme, and grid partitioning is achieved through a scalable pencil decomposition approach. Subgrid-scale stresses are modeled with a standard Smagorinsky model with wall damping. Wind turbines are modeled by an actuator sector model, coupled with a nonlinear flexible multi-body dynamics model.

Turbulent inflow conditions for wind-farm simulations are generated in separate precursor simulations (see, e.g. Munters, Meneveau & Meyers 2016). A streamwise slab of the velocity and temperature field is stored to disk when running the precursor, and is later introduced in the wind-farm domain by means of body forces in a so-called fringe region.

4.2.2. ELLIPSYS-3D (DTU)

EllipSys-3D is a general-purpose flow solver (Michelsen 1992, Sørensen 1994), solving the discretized incompressible Navier–Stokes equations in general curvilinear coordinates using a block-structured finite-volume approach. Pressure coupling is achieved using the SIMPLE algorithm with Rhie-Chow momentum interpolation. The convective terms are discretized with fourth order central differences (CDS4). The subgrid-scale stresses are here modeled with the model by Deardorff (1972). The turbines are modeled using the actuator line method(Sørensen and Shen 2002), which have been fully coupled to the aero-elastic tool, Flex5 (Øye 1996).

Turbulent inflow is also generated in separate precursor simulations, where the velocities are extracted at a given plane in the domain and saved for later use. These will be introduced directly on the inflow boundary in the simulations of wind-farms.

4.3. SIMULATION DOMAINS AND NUMERICAL SETUP

The simulation domain has a size of $16 \times 16 \times 1.5\ \mathrm{km}^3$ in the streamwise, spanwise, and vertical directions respectively (see Figure 3). This size is a compromise between having a small blockage of the turbines in the domain (in the eventual upcoming wind farm simulations) and keeping computational costs reasonable. Grid resolutions are slightly different for the two simulation platforms. The grid resolution for SP-Wind is chosen to be $13.33 \times 13.33 \times 6.66\ \mathrm{m}^3$, resulting in a computational grid of $1200 \times 1200 \times 225 = 324 \times 10^6$ gridpoints. The grid resolution for EllipSys3D is generally $20 \times 20 \times 10\mathrm{m}^3$, although the mesh is stretched for the upper 500m. This gives a total of $800 \times 800 \times 128 = 82 \times 10^6$ gridpoints.

Figure 3 shows a typical precursor flow field at hub height, indicating that the domain size is large enough to encompass several instances of the large streamwise-elongated structures in the turbulent flow.

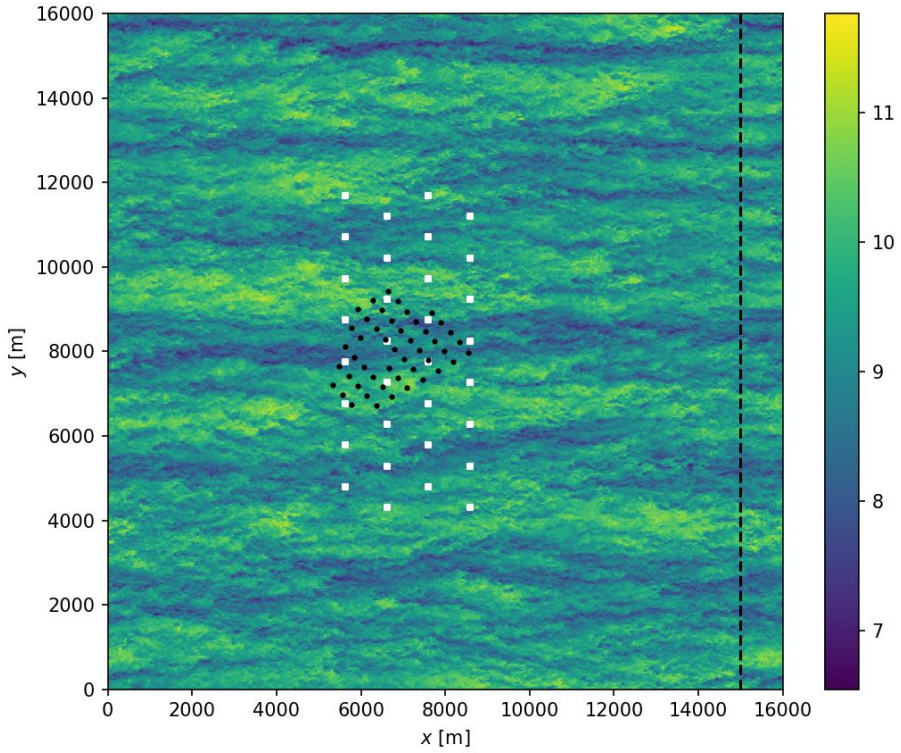

Figure 3: Planview of Lillgrund (black) and TotalControl Reference windfarm layout (white) in simulation domain. The black dashed line indicates the extent of the slab from which inflow data is extracted from the precursor simulation (without turbines). The background is colored with a typical instantaneous streamwise velocity field at turbine hub height in a precursor simulation without turbines.

Wind-farm simulations are performed in a sequence of steps. Firstly, a fully-developed turbulent boundary layer is generated in a so-called *spinup* simulation with periodic boundary conditions but without turbines. This spinup simulation is initialized with a given boundary layer profile, upon which random divergence-free perturbations are imposed. The flow is advanced for a time period of 20 hours, after which spurious effects of the random perturbations have disappeared, and the flow has reached a fully-developed and statistically stationary state. Furthermore, EllipSys3D employs grid sequencing to decrease the total computational time. Grid sequencing allows larger time steps on a coarser grid during the initial stages of the spinup as the initial stages are performed on a coarser grid level, before jumping to a finer and finer grid resolution. A total of three different grid levels are used for the grid sequencing.

Next, the obtained flow field is advanced in time using a *precursor* simulation (also with periodic boundary conditions) to generate time series of unsteady turbulent inflow conditions. The precursor simulations are performed for a time span of 75 minutes, as a compromise between obtaining a time series long enough for converged statistics on the one hand, and keeping disk storage requirements manageable on the other.

Eventually, data from the precursor simulations can be fed as inflow conditions to a set of wind-farm large-eddy simulations. As discussed above, these latter simulations are not further discussed here, and will be described in a follow-up report. The general domain and time parameters discussed in the current and previous paragraph are summarized in *Table 1*.

*Table 1: General domain parameters. * The grid for EllipSys3D is stretched for the upper 500m. §The smallest time step on the finest grid level.*

	Variable	SP-Wind	EllipSys3D
Domain size	$L_x \times L_y \times L_z$	$16 \times 16 \times 1.5$ km³	$16 \times 16 \times 1.5$ km³
Grid	$N_x \times N_y \times N_z$	$1200 \times 1200 \times 225$	$800 \times 800 \times 128$
Resolution	$\Delta_x \times \Delta_y \times \Delta_z$	$13.33 \times 13.33 \times 6.66$ m³	$20 \times 20 \times 10^*$ m³
Spinup time	T_{spin}	20 h	20 h
Precursor time	T	75 min	60 min
Time step	Δt	0.5 s	0.8 s – 1.0§ s

5. PRESSURE-DRIVEN BOUNDARY LAYER CASES

Fully-developed canonical pressure-driven boundary layers (PDBLs, alternatively half-channel flows in literature) at high Reynolds numbers have been used since long as simplified surrogates for an actual atmospheric boundary layer flow (see, e.g., Ivanell et al. (2007); Calaf et al. (2010)). The governing equations are simplified from the ABL equations shown above by omitting the equation for temperature θ as well as any terms related to Coriolis forces and thermal buoyancy, resulting in

$$\nabla \cdot \tilde{\boldsymbol{u}} = 0$$

$$\frac{\partial \tilde{\boldsymbol{u}}}{\partial t} + (\tilde{\boldsymbol{u}} \cdot \nabla)\tilde{\boldsymbol{u}} = -\nabla(\tilde{p} + p_\infty)/\rho \; - \nabla \cdot \boldsymbol{\tau}_s + \boldsymbol{f}$$

5.1. CASE DESCRIPTION

Spinups are initialized with a mean logarithmic velocity profile, upon which random divergence-free perturbations are added. These initial conditions are then advanced in time for 20 physical hours, so that the influence of the unphysical perturbations has disappeared, and the flow has reached a fully turbulent and statistically stationary state.

5.1.1. SIMULATION PARAMETERS

The rough-wall turbulent boundary layer has a mean-flow profile $U(z)$ following the log-law

$$U(z) = \frac{u_*}{\kappa} \ln \frac{z}{z_0}$$

with κ the Von Karman constant and $u_* = \sqrt{-H/\rho \; \nabla p_\infty}$ the friction velocity. Simulations are performed for a typical friction velocity in offshore boundary layers of $u_* = 0.28$ m/s, which requires a driving pressure gradient $\nabla p_\infty/\rho = -5.2267 \times 10^{-5}$ m/s^2. The dataset contains a base case with a standard offshore roughness length of 2×10^{-4} m, performed by both SP-Wind and EllipSys3D. Furthermore, two cases with a higher and lower roughness length z_0 of 2×10^{-3} m, and 2×10^{-5} m are performed, resulting in a different turbulence intensity at turbine height.

Table 2: PDBL setup parameters

Simulation parameters		
Friction velocity	u_*	$0.28\ \mathrm{m/s}$
Driving pressure gradient	$\nabla(p_\infty)/\rho$	$-5.2267 \times 10^{-5}\ \mathrm{m/s^2}$
Simulation cases		
PDk	KU Leuven	$z_0 = 2 \times 10^{-4}\ \mathrm{m}$
PDd	DTU	$z_0 = 2 \times 10^{-4}\ \mathrm{m}$
PDkhi	KU Leuven	$z_0 = 2 \times 10^{-3}\ \mathrm{m}$

5.1.2. GENERALIZATION & RESCALING

When non-dimensionalizing with the correct scaling parameters, different pressure-driven boundary layers for varying flow conditions collapse due to similarity. Vice versa, the current dataset can be generalized to different flow conditions by rescaling the flow variables by these same parameters. In that sense, after proper rescaling one case covers an entire range of possible wind speeds and roughness lengths.

Firstly, it is well known that the appropriate velocity scaling is the friction velocity u_*, and hence different wind speeds can be attained by rescaling the entire flow field by a different friction velocity u_*^{new}. Second, for rough-wall boundary layers at high Reynolds numbers in which the roughness elements are much smaller than the boundary-layer height (it is the case for offshore atmospheric boundary layers), the roughness acts merely to increase surface stress without any structural changes in the flow (Jimenez 2004, Castro 2007), in line with the classical outer layer similarity hypothesis (Townsend 1976). The effect of a different roughness length z_0^{new} can be captured by imposing an offset on the mean flow in line with the difference in roughness. Hence, denoting the imposed friction velocity and roughness length in the current cases by u_*^{old} and z_0^{old} respectively, the flow can be rescaled as

$$\boldsymbol{u}'^{,new} = \boldsymbol{u}'^{,old}\,\frac{u_*^{new}}{u_*^{old}},$$

$$\boldsymbol{U}^{new} = \boldsymbol{U}^{old}\,\frac{u_*^{new}}{u_*^{old}} + \frac{1}{\kappa}\ln\frac{z_0^{old}}{z_0^{new}},$$

for the fluctuating components and mean flow respectively.

5.2. PRECURSOR SIMULATION RESULTS

In this section sample results in the form of time-averaged flow profiles are shown. More details and time series are provided in the full database, described in Section 7.

First, results of the KU Leuven simulations are discussed. Figure 4 below shows flow profiles for the PDBL cases, averaged horizontally and in time. The left figure depicts the mean-flow velocity profile, which shows good correspondence with log-law behavior for both cases with their respective wall roughness up until $z/\delta \approx 0.2$, as can be expected. The right figure shows turbulence kinetic energy (TKE) and Reynolds shear stress, which are shown to be virtually independent of the wall roughness, in accordance to Townsend's outer layer similarity hypothesis. Time-averaged spectra of streamwise velocity are shown in Figure 5. Spectral behavior of velocity fluctuations is also shown to be independent of wall roughness, except for some discrepancies in the low wavenumber spanwise spectra, which can be attributed to lack of statistical convergence for the given time horizon.

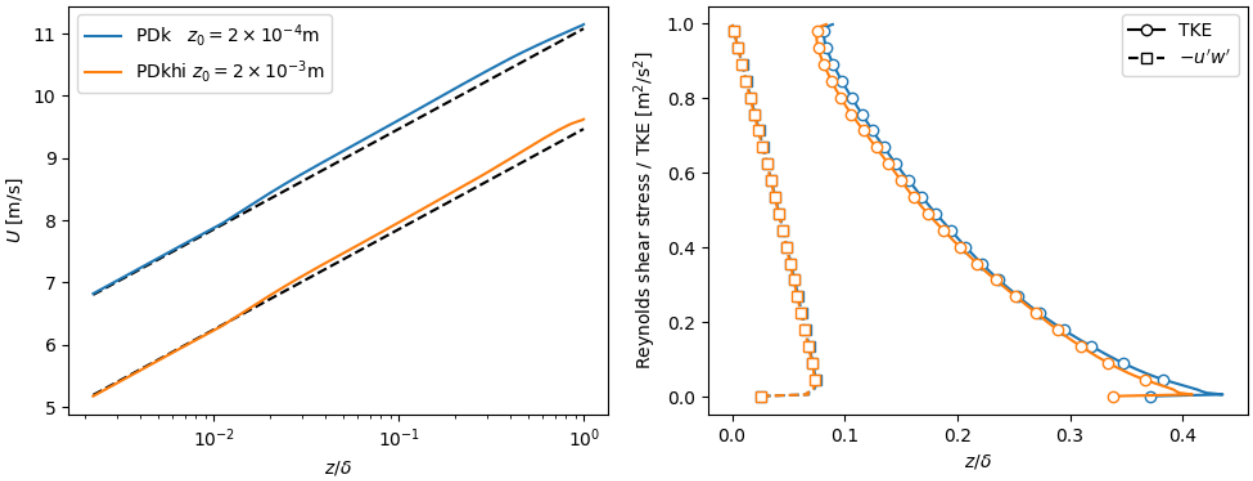

Figure 4: Flow profiles for PDBL cases of KU Leuven. Left: Mean velocity. Dashed lines indicate log-law profiles. Right: resolved Reynolds shear stress and turbulent kinetic energy

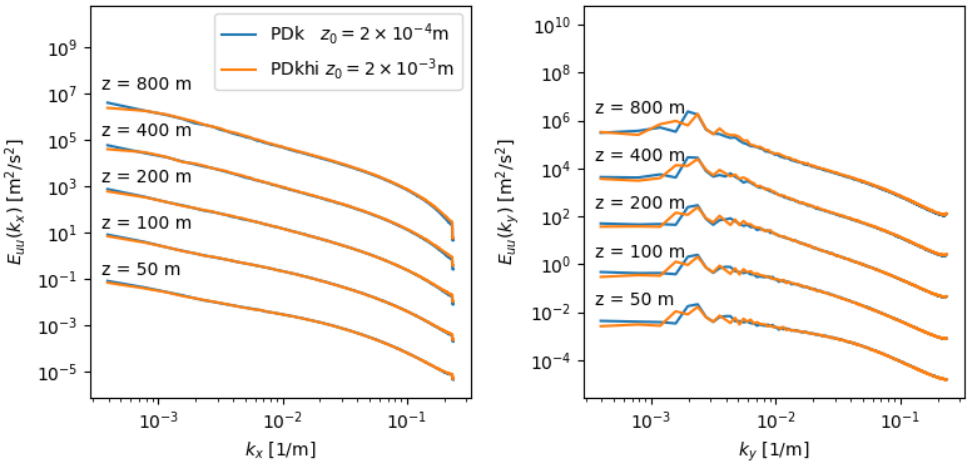

Figure 5: Time-averaged spectra of streamwise velocity at different heights for KU Leuven simulations. Left: Streamwise spectra, averaged over spanwise direction. Right: Spanwise spectra, averaged over streamwise direction. Spectra are shifted vertically for clarity of presentation.

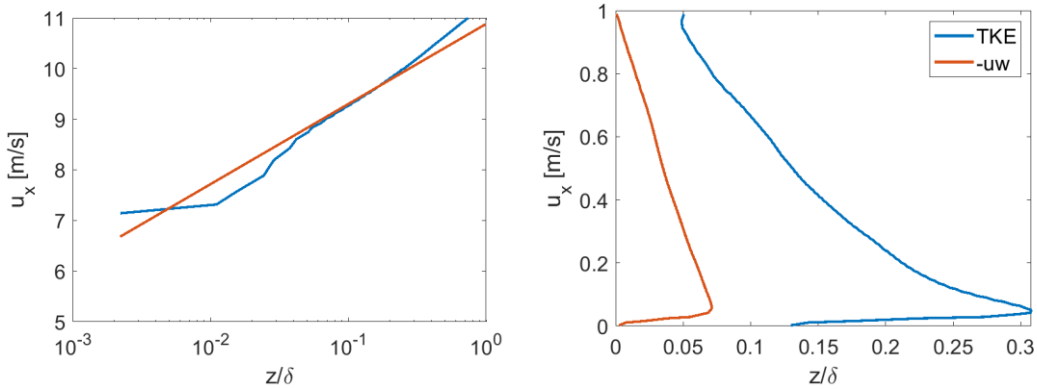

Figure 6: Flow profiles for PDBL case by DTU. Left: Mean velocity. Red line indicates log-law profile. Right: resolved Reynolds shear stress and turbulent kinetic energy

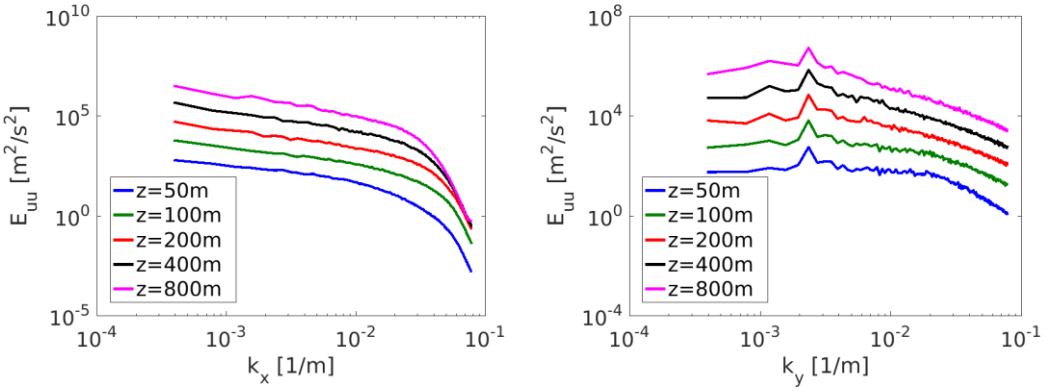

Figure 7: Spectra of streamwise velocity at different heights for DTU simulations. Left: Streamwise spectra, averaged over spanwise direction. Right: Spanwise spectra, averaged over streamwise direction. Spectra are shifted vertically for clarity of presentation.

The corresponding results from the DTU case are shown in Figure 6 and Figure 7. The mean velocity profile deviate more from the log-law than the predictions of KU Leuven, which is primarily due to the coarser grid resolution. However, in the region around hub height and a few hundred meters above the predicted slope follows closely the expected log-law. Note that the log-law results are based on a friction velocity of 0.275 m/s instead of 0.28 m/s. The offset is due to the simulations not being fully stationary This is because the simulated results are still undergoing slow transients and therefore are not fully converged. The trends of the turbulence quantities are the same as those predicted by KU Leuven. The lower resolved turbulence level is due to the coarser grid resolution. The spectra computed by DTU are similar to those of KU Leuven but obviously do not resolve the small scales as well. Again this can be traced back to the grid resolution.

6. Conventionally-neutral Atmospheric Boundary Layer Cases

The current section discusses the definition and results of the conventionally neutral atmospheric boundary layer cases (CNBLs). The conventionally neutral boundary layer consists of a neutral boundary layer, capped by a strongly stable inversion layer. Above the CNBL, the free atmosphere is stably stratified with a constant potential temperature gradient.

Such a boundary layer can form, for instance, with wind blowing from onshore to the sea in daytime during spring (when the sea surface temperature is still relatively cold). The change in surface roughness and heat flux will cause a growing stable internal boundary layer, which eventually results in a neutral boundary layer capped by a stable inversion layer.

6.1. Case description

The simulation cases included in the current dataset are designed based on similar precursor cases for wind-farm LES discussed in Allaerts & Meyers (2017). Cases are forced with a constant geostrophic wind speed of $G = 12\ \mathrm{m/s}$ and the base wall roughness length is $z_0 = 2 \times 10^{-4}\ \mathrm{m}$. The lapse rate in the stably-stratified free atmosphere is $\gamma = 1\ \mathrm{K/km}$, and the temperature of the mixed layer is $\theta_m = 15°$, which is also taken as the reference temperature. The Coriolis parameter is $f_c = 10^{-4}\ \mathrm{s}^{-1}$, corresponding to a latitude of $43.43°$.

In contrast to the PDBL cases where the boundary layer extends to the top of the domain, in the CNBL cases, the height of the boundary layer will result from a balance between entrainment on the one hand and a stably stratified free atmosphere and capping inversion on the other. An empirical formula for this height h is given by

$$h = A\frac{\theta_0}{g\Delta\theta}u_*^2,$$

with $A \approx 500$ an empirical parameter and $\Delta\theta$ the strength of the capping inversion.

In order to limit the computational cost of spinning up statistically stationary boundary layers, the initialization of both temperature and velocity fields is performed with care based on the procedure described in Allaerts & Meyers (2015), and Rampanelli & Zardi (2004). The temperature profile is initialized as

$$\theta(z) = \theta_m + (\Delta\theta + \gamma\Delta h/3)\frac{\tanh(\eta)+1}{2} + \gamma\Delta h/3\ \frac{\ln(2\cosh(\eta))+\zeta}{2},$$

with $\Delta h = 100$ m the initial thickness of the capping inversion, and $\eta = (z-h)/(\Delta h/3)$ a dimensionless height. This profile allows a smooth transition between a mixed (constant) temperature below the inversion and a stably stratified profile in the free atmosphere. The velocity profile is initialized by blending together two functions representing the boundary layer and free atmosphere profiles. In the free atmosphere, the velocities $u_\uparrow = G\cos\alpha$ and $v_\uparrow = G\sin\alpha$ are simply initialized to the geostrophic velocity G at an appropriate angle. Below the capping inversion, velocities are initialized as

$$u_\downarrow = (u_*/\kappa)\,[\ln(z/z_0) + f_u(\zeta)]$$
$$v_\downarrow = -(u_*/\kappa)f_v(\zeta)\ \mathrm{sign}\ f_c,$$

With $\zeta = z_0/h$, $f_u = 1.57\,\zeta - 2.68\zeta^2$, and $f_v = 13.2\zeta - 8.7\zeta^2$. Finally, velocity profiles above and below the capping inversion are merged smoothly using a tanh function as

$$\boldsymbol{u} = \boldsymbol{u}_\downarrow\frac{1-\tanh[(\zeta-0.5)2h_0/\Delta h]}{2} + \boldsymbol{u}_\uparrow\frac{1+\tanh[(\zeta-0.5)2h_0/\Delta h]}{2},$$

with $h_0 = h - \Delta h/2$ the bottom of the capping inversion. These mean velocity profiles are then rotated such that the velocity vector is pointing in the x direction at a height of $z = 119$ m (i.e. the hub height of the DTU 10 MW reference turbine. Furthermore, random divergence-free Fourier perturbations with an amplitude of $0.1G$ are added below 100 m to provoke the development of turbulence, and simulations are advanced in time by 20 hours before gathering precursor data. During the entire spinup and precursor process, a wind angle controller is used to keep a wind direction along the domain x axis at $z = 119$ m (corresponding to the hub height of the wind turbines in the upcoming wind-farm simulations). This controller is turned off for the actual wind-farm simulations.

KU Leuven will focus on varying the boundary layer height by choosing different capping inversion strengths ($\Delta\theta = 2\ \mathrm{K}, 4\ \mathrm{K}$) in two simulation cases with estimated equilibrium boundary layers at 500 m, and 250 m respectively. DTU will focus on different inflow turbulence intensities by varying the wall roughness, only one roughness has been finalized so far due to limited computational resources. Simulation parameters are summarized in *Table 3*.

The initial conditions for the mean wind velocity vector along the domain height as well as the temperature are shown for the CNk2 and CNk4 cases in *Figure 8.* The figure shows the smooth transition between the velocities and temperatures in the boundary layer (characterized by veered and sheared velocities with well-mixed temperature) and in the free atmosphere above the capping inversion (with uniform velocities and stable free-atmosphere stratification).

Table 3: CNBL simulation parameters

Simulation parameters			
Geostrophic wind		G	$12\ \mathrm{m/s}$
Coriolis parameter		f_c	$10^{-4}\ \mathrm{s}^{-1}$
Simulation cases			
CNk2	KU Leuven		$z_0 = 2\times10^{-4}\ \mathrm{m}, \Delta\theta = 2\mathrm{K}\ (h = 500\ \mathrm{m})$
CNk4	KU Leuven		$z_0 = 2\times10^{-4}\ \mathrm{m}, \Delta\theta = 4\mathrm{K}\ (h = 250\ \mathrm{m})$
CNd	DTU		$z_0 = 2\times10^{-4}\ \mathrm{m}, \Delta\theta = 2\mathrm{K}\ (h = 500\ \mathrm{m})$

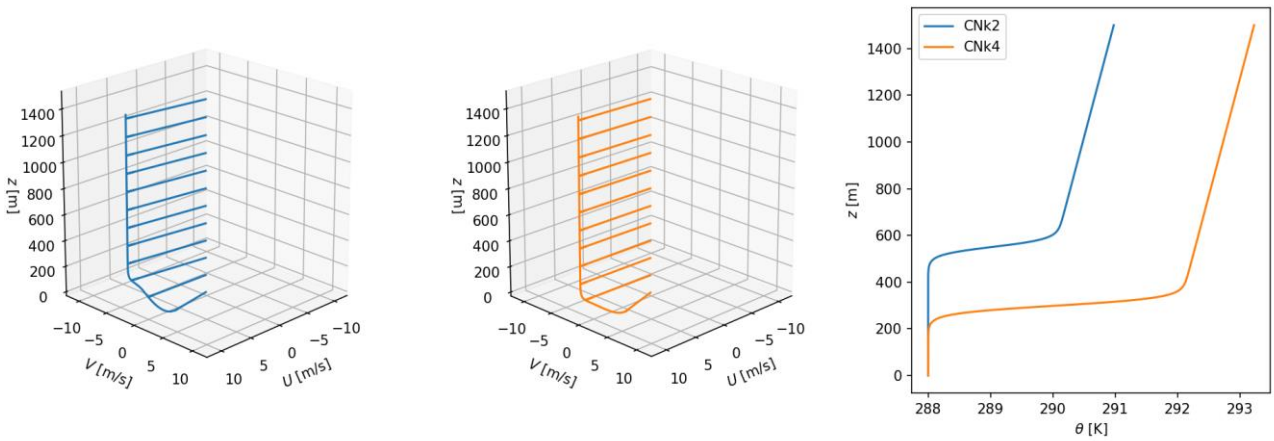

Figure 8: Initial profiles for velocity (left: CNk2, Middle: CNk4) and temperature (Right)

6.2. PRECURSOR SIMULATION RESULTS

Similar to the PDBL cases discussed above, the current section showcases some examples of low-dimensional flow data. Details of the publicly available dataset are discussed below in Section 7.

Figure 9 illustrates flow profiles for the KU Leuven CNBL cases. The inclusion of Coriolis and buoyancy forces with a capping inversion and stable free-atmosphere stratification results in a flow with significantly more complex features than the canonical PDBL cases described above. The flow is split into a turbulent atmospheric boundary layer below the capping inversion, and a shear-free non-turbulent free-atmosphere flow above. In the boundary layer, significant veer is observed, which is strong for CNk4 with its lower boundary layer height and stronger inversion strength. Furthermore, the top left panel shows that a supergeostrophic jet is formed at the top of the boundary layer. These observations coincide with those found in Allaerts & Meyers.

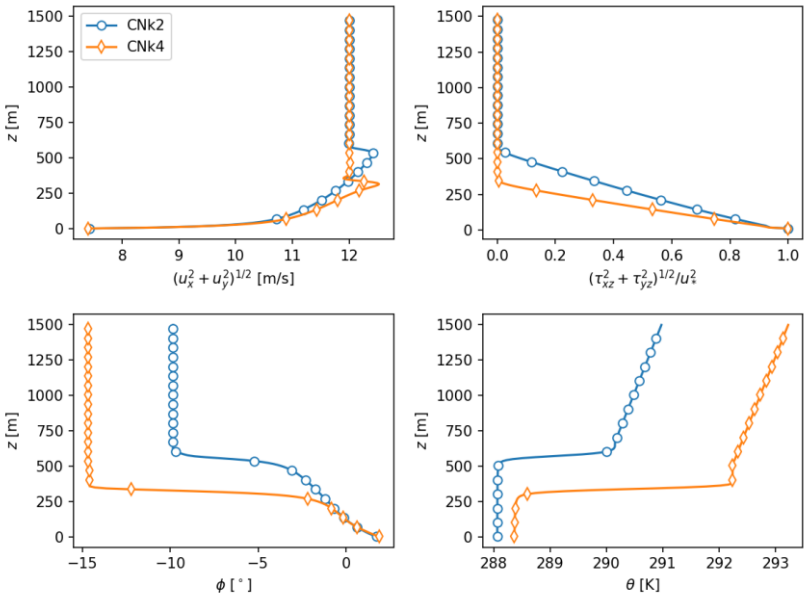

Figure 9: Flow profiles for KU Leuven CNBL cases with varying boundary layer heights. Top left: Horizontal velocity. Top right: Total (resolved + subgrid) shear stress. Bottom left: Wind veer. Bottom right: Potential temperature.

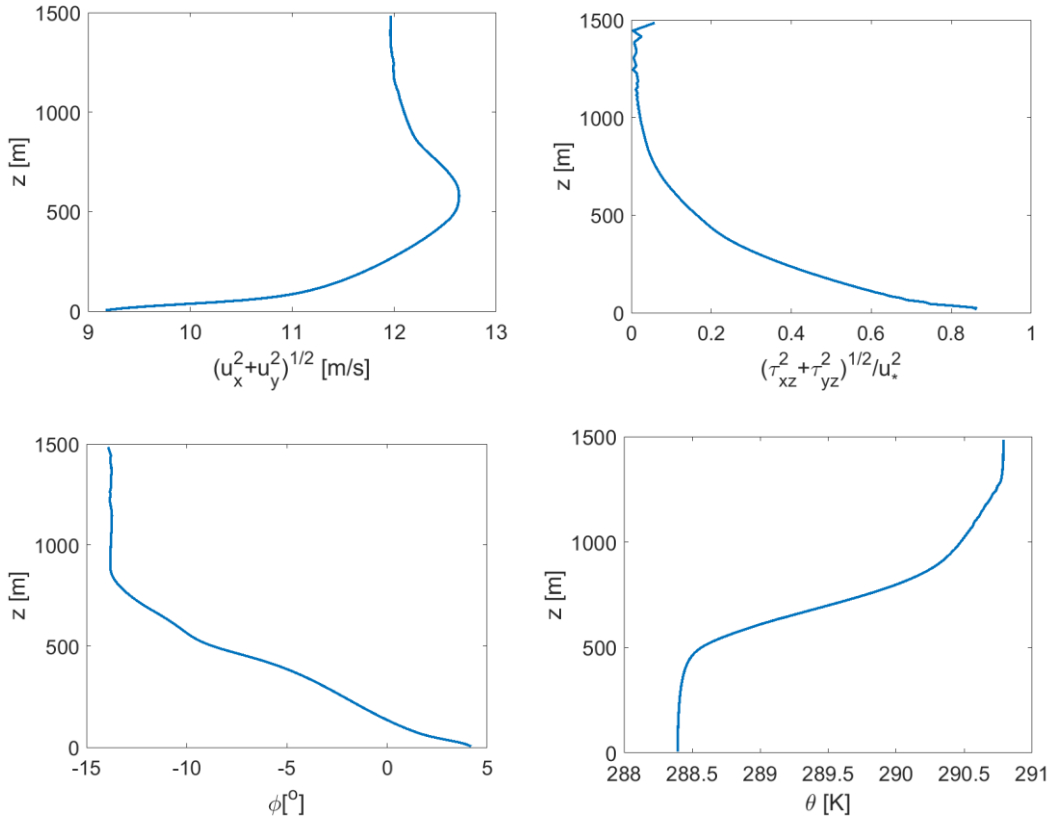

Figure 10: Flow profiles for DTU CNBL cases with varying boundary layer heights. Top left: Horizontal velocity. Top right: Total (resolved + subgrid) shear stress. Bottom left: Wind veer. Bottom right: Potential temperature.

The results of the CNBL case simulated by DTU are shown in Figure 10. The trends are the same as found by KU Leuven but there are important differences. The supergeostrophic jet predicted by DTU is not as distinct which is primarily due to the coarser grid resolution used by DTU. Furthermore, the shear stress undergoes some unexpected wiggles near the top of the domain. Again this can partly be attributed to the coarser grid combined with the use of a CDS4 scheme for the convective terms. However, another reason is that the simulation assumes symmetry conditions on all variables at the top boundary. This causes the gradient of the temperature profile to approach zero in the vicinity of the upper boundary and hence removes the otherwise damping effect of the positive temperature gradient. In simulations with higher domains and finer grid resolution the use of symmetry conditions for the temperature is normally not an issue because all turbulence then is already dampened out and because the shear is zero then production of turbulence is zero. The wiggles are in part also due to oscillation in the horizontal averaged vertical velocity. Unlike many pseudo-spectral codes EllipSys3D does not force the horizontal averaged vertical velocity to zero. In effect the horizontal averaged vertical velocity may oscillate around zero when the grid is coarse.

7. ACCESS TO DATASETS

The full data from the KU Leuven precursor simulations is stored on an archiving system of the Flemish Supercomputer Center at KU Leuven. The entire dataset consists of a set of time-averaged flow variables, snapshots of the flow field, and the full spatio-temporal solution field in the fringe region (see *Figure 3*). The latter is necessary to run the upcoming wind-farm simulations and takes up most of the disk storage requirements, which total up to roughly 50 TB.

A subset of this dataset is publicly available in the form HDF5 files hosted on a community of Zenodo repositories at : https://zenodo.org/communities/totalcontrolflowdatabase/. Additional virtual flow measurements can be made available upon request. The data is split up into three files (precursor_snapshot.h5, precursor_timeavg.h5, and precursor_timeseries.h5) in order to keep the size of each file relatively small. More specifically, the dataset consists of:

Snapshots: precursor_snapshot.h5, ~5GB

- A snapshot of the full velocity (+ temperature) field at t = 75 min

Time averages: precursor_timeavg.h5, ~5MB

- Velocity spectra
  - Streamwise spectra at every height, averaged over spanwise direction
  - Spanwise spectra at every height, averaged over streamwise direction
- Profiles
  - Velocity components (+ temperature)
  - Reynolds stresses

Time series: precursor_timeseries.h5, ~5GB

- Virtual met mast data of velocity components (+temperature) at $(x, y) = (16\ \mathrm{km}, 0\ \mathrm{km})$ at 2 Hz resolution
- Cross section (yz) of velocity components (+temperature) at x = 16 km at 0.2 Hz resolution
- 3D box at $x \times y \times z = [15.9 \ldots 16] \times [0 \ldots 0.1] \times [0 \ldots 0.5]\ \mathrm{km}^3$ at 0.2 Hz resolution

The data repository contains a Python script read_inflow.py which can be used to import, manipulate and visualize the data. An example visualization of the provided script is included in the figures below.

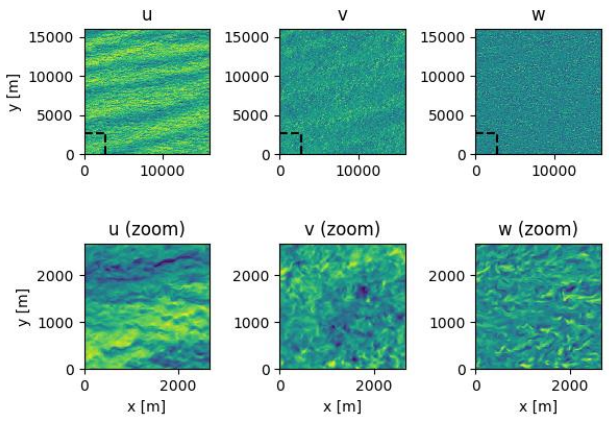

Figure 11: Snapshot of velocity components at z = 100 m for case CNk4 (from precursor_snapshot.h5)

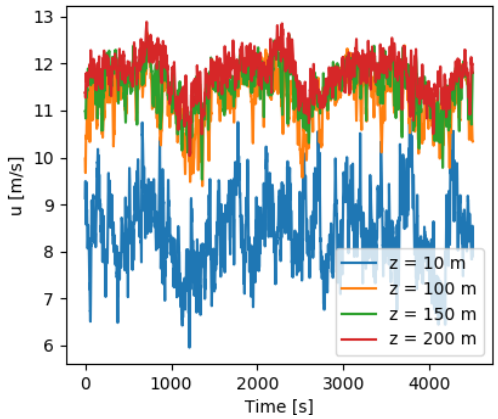

Figure 12: Metmast streamwise velocity data for case CNK4 (from precursor_timeseries.h5)

Similarly, the data from the EllipSys3D precursor simulations are stored on the local DTU Wind Energy cluster. The data will also be uploaded to the Zenodo repository with the necessary scripts to read and postprocess the data, once some minor issues have been sorted out.

8. Conclusion

In the current document, the first part of deliverable D1.04 of the TotalControl project was discussed consisting of the precursor simulations and resulting database necessary for the full wind-farm simulations envisaged in the proposal. Two different simulation codes were used, i.e. SP-Wind of KU Leuven and EllipSys-3D of DTU. Three pressure driven boundary layers with two different surface roughness are included. Next to that, three conventionally neutral boundary layers, with two different (stable) stratification strengths in the capping inversion were considered, leading to two different boundary layer heights. All date is stored on the supercomputing facilities of KU Leuven and DTU, and subsets are made publically available (the full data set is too large for this)

The current report constitutes the first part of D1.04, but is fully in line with the measure of success envisaged for D1.04, i.e. "*complete data base covering detailed wind field and WPP operation parameters for different atmospheric conditions (e.g. stability classes) and transients, publically available.*" At this point full flow databases are available. We remark here that our focus with respect to stability classes has shifted from considering stable/unstable stratification near the surface (as relevant in most onshore scenarios) to different stratification strengths of the capping inversion, which is particularly relevant and interesting for offshore conditions, and fully in line with the focus on large offshore wind farms of the TotalControl project. Finally, the second part of D1.04, which uses the current precursor data as inflow data for wind-farm simulations with the reference wind farm for different scenarios (inflow directions, wind-farm transients, etc.) is estimated to appear by the end of 2019, i.e. Month 24 of the TotalControl project.

9. References

Allaert D. & Meyers J. (2015). Large eddy simulation of a large wind-turbine array in a conventionally neutral atmospheric boundary layer. *Physics of Fluids* **27**, 065108.

Allaerts D. & Meyers J. (2017). Boundary-layer development and gravity waves in conventionally neutral wind farms. *Journal of Fluid Mechanics* **814**, 95 – 130.

Andersen, S. J., Madariaga, A., Merz, K., Meyers, J., Munters, W., & Rodriguez, C. (2018). Reference Wind Power Plant D1.03. DTU Technical Report.
Online available at: http://orbit.dtu.dk/files/164663085/TotalControl_D1_03_Reference_Wind_Farm.pdf

Bak C. et al. (2013). The DTU 10-MW Reference Wind turbine. DTU Technical Report.
Online available at: http://dtu-10mw-rwt.vindenergi.dtu.dk/

Calaf M., Meneveau C. & Meyers J. (2010). Large eddy simulation study of fully developed wind-turbine array boundary layers. *Physics of Fluids* **22**, 015110.

Castro I. P. (2007). Rough-wall boundary layers: mean flow universality. *Journal of Fluid Mechanics* **585**, 469 – 485.s

Deardorff, J.W., 1972: Numerical Investigation of Neutral and Unstable Planetary Boundary Layers. *J. Atmos. Sci.*, **29**, 91–115.

Ivanell S., Sørensen J.N. & Henningson D. (2007). Numerical computations of wind turbines wakes. Berlin: Springer.

Jimenez J. (2004). Turbulent Flows over Rough Walls. *Annual Review of Fluid Mechanics* **36**: 173 – 96.

Michelsen, J. A.: Basis3D - a platform for development of multiblock PDE solvers., Tech. Rep. AFM 92-05, Technical University of Den-mark, Lyngby, Denmark, 1992.

Munters W. & Meyers J. (2018). Optimal dynamic induction and yaw control of wind farms: effects of turbine spacing and layout. Journal of Physics: Conference Series, 0320125.

Munters W., Meneveau C. & Meyers J. (2016). Turbulent inflow precursor method with time-varying direction for large-eddy simulations and applications to wind farms. Boundary-layer Meteorology, 305 – 328.

Rampanelli G. & Zardi D. (2004). A Method to Determine the Capping Inversion of the Convective Boundary Layer. Journal of Applied Meteorology 43, 925 – 933.

Sørensen, J. N. and Shen, W. Z.: Numerical modeling of wind tur-bine wakes, Journal of fluids engineering, 124, 393–399, 2002.

Sørensen, N. N.: General purpose flow solver applied to flow over hills, Ph.D. thesis, Risø National Laboratory, Roskilde, Denmark, 1994.

Townsend, A. A. R. (1976). The Structure of Turbulent Shear Flow. Cambridge University Press.

Øye, S.: FLEX4 simulation of wind turbine dynamics, in: Proceed-1oings of the 28th IEA Meeting of Experts Concerning State of theArt of Aeroelastic Codes for Wind Turbine Calculations (Avail-able through International Energy Agency), 1996.